



## An improved, time-efficient approach to extract accurate distance restraints for NMR<sup>2</sup> structure calculation.

Aditya Pokharna<sup>a</sup>, Felix Torres<sup>a</sup>, Harindranath Kadavath<sup>a</sup>, Julien Orts<sup>\*b</sup>, and Roland Riek<sup>\*a</sup>

<sup>a</sup>Laboratory of Physical Chemistry, ETH, Swiss Federal Institute of Technology, HCI F217, Vladimir-Prelog-Weg 2, 8093 Zürich, Switzerland

<sup>b</sup>University of Vienna, Faculty of Life Sciences, Department of Pharmaceutical Sciences, Althanstrasse 14, 2F 353, A-1090, Vienna, Austria

\*Correspondence to : Roland Riek (roland.riek@phys.chem.ethz.ch) and Julien Orts (julien.orts@univie.ac.at)

### Abstract

1  
2  
3  
4  
5  
6  
7  
8  
9  
10  
11  
12  
13  
14  
15  
16  
17

Exact Nuclear Overhauser Enhancement (eNOE) yields highly accurate, ensemble averaged <sup>1</sup>H-<sup>1</sup>H distance restraints with an accuracy of up to 0.1 Å for the multi-state structure determination of proteins as well as for Nuclear Magnetic Resonance Molecular Replacement (NMR<sup>2</sup>) to determine the structure of the protein-ligand interaction site in a time-efficient manner. However, in the latter application, the acquired eNOEs lack the obtainable precision of 0.1 Å because of the asymmetrical nature of the filtered NOESY experiment used in NMR<sup>2</sup>. This error is further propagated to the eNOE equations used to fit for and extract the distance restraints.

In this work, a new analysis method is proposed to obtain inter-molecular distance restraints from the filtered NOESY spectrum more accurately and intuitively by dividing the NOE cross-peak by the corresponding diagonal peak of the ligand. The method termed diagonal-normalized eNOEs was tested on the data acquired by Torres et al. (Torres et al., 2020) on the complex of PIN1 and a small, weak-binding phenylimidazole fragment. The diagonal-normalised eNOE derived distance restraints NMR<sup>2</sup> yielded the right orientation of the fragment in the binding pocket, and produced a structure that more closely resembles the benchmark X-ray structure (2XP6) (Potter et al., 2010) with an average heavy atom RMSD of 1.681 Å than the one produced with traditional NMR<sup>2</sup> with an average heavy atom RMSD of 3.628 Å, attributed to the higher precision of the evaluated distance restraints .



18 1 INTRODUCTION

19 Nuclear Magnetic Resonance Molecular Replacement (NMR<sup>2</sup>) is a hybrid approach to determine the structure  
20 of protein-ligand complexes, utilising a previously determined structure (for example, a X-ray structure or  
21 a structure from a protein homolog) of the target protein and combining it with the spatial information  
22 extracted by solution state NMR to identify the binding pocket of the protein and the orientation of the ligand  
23 inside it (Wälti and Orts, 2018). The major strength of the method is that one does not need to carry out  
24 protein resonance assignment to obtain the complex structure. Using NMR<sup>2</sup>, Orts et al. has been able to solve  
25 the structure of various complexes (Torres et al., 2020); (Wälti and Orts, 2018); (Orts et al., 2016) accurately  
26 (up to 1 Å) within a few days of measurement and analysis. The NMR<sup>2</sup> structure calculation workflow is  
27 detailed in (Orts and Riek, 2020) and relies on acquiring precise inter-molecular distance restraints.

28 In NMR<sup>2</sup>, the <sup>13</sup>C, <sup>15</sup>N-labelled protein and non-labelled ligand are mixed and measured together using  
29 the F<sub>1</sub>-[<sup>15</sup>N, <sup>13</sup>C]-filtered [<sup>1</sup>H, <sup>1</sup>H]-NOESY experiment (Zwahlen et al., 1997) to extract the inter-molecular  
30 NOE rates and the corresponding distances. This analysis is performed in an in-built module within CYANA  
31 structure calculation software (Güntert and Buchner, 2015) called ENORA (Strotz et al., 2017). ENORA fits  
32 the NOE buildup curves obtained at multiple mixing times to extract exact cross-relaxation rates (eNOEs)  
33 which produces semi-accurate distance restraints with both upper and lower limit (Vögeli et al., 2009).

34 However, the precision of these inter-molecular distance restraints is much lower (~20% higher tolerance  
35 needed) (Strotz et al., 2015) than the bi-directional intra-molecular eNOEs, usually measured inside the  
36 protein, from a series of <sup>15</sup>N, <sup>13</sup>C-resolved [<sup>1</sup>H, <sup>1</sup>H]-NOESY experiments that have a precision of 0.1 Å. The  
37 lower precision is attributed to the imbalanced magnetisation pathway within the F<sub>1</sub>-<sup>15</sup>N, <sup>13</sup>C-filtered [<sup>1</sup>H, <sup>1</sup>H]-  
38 NOESY experiment, the lack of a clean steady state magnetisation at the beginning of the experiment, the  
39 unknown spin diffusion contribution (Kalk and Berendsen, 1976) and the complexity involved in extracting  
40 distances within ENORA, which further propagates errors arising from the NOESY spectrum.

41 In this work, we present an alternative approach for extracting cross-relaxation rates from the filtered  
42 2D NOESY spectra that forgoes the need for the sophisticated and time-intensive eNORA calculations and  
43 produces more accurate distances. The complex used in this study is that of cis/trans isomerase PIN<sub>1</sub>  
44 with a low molecular weight fragment, 4-Methyl-2-(3-methylphenyl)-1H-imidazole-5-carboxylic acid, whose  
45 structure of the interaction site was solved by Torres et. al (Torres et al., 2020), in order to test the NMR<sup>2</sup>  
46 method for weak binding small molecules. This fragment called Compound 1 in the paper by Torres et al.  
47 (Torres et al., 2020) produces very few inter-molecular eNOEs to PIN<sub>1</sub>, due to its small size (comprising only  
48 a few protons) and low binding affinity (260 μM). This makes the de-novo determination of the right pose of  
49 the ligand in the binding pocket using NMR<sup>2</sup> very challenging.

50 As we shall see, our approach has been successful in producing better restraints for the PIN<sub>1</sub>-Compound  
51 1 complex than the standard procedure thereby predicting the right orientation of the ligand in the binding  
52 pocket when compared with the X-ray structure of this complex (2XP6) (Potter et al., 2010), which serves as  
53 a benchmark to ascertain the accuracy of the NMR<sup>2</sup> structures.

54 2 THEORY

55 Following the standard NMR theory of the NOESY experiment (Keepers and James, 1984), the proposed  
56 analysis arises out of simple approximations made on the fundamental equations used to calculate eNOEs.  
57 Every spin pair that produces a cross-peak can be assumed to form a two-spin system. The cross-relaxation  
58 rate for a two-spin system (i and j) can be analytically given as (Vögeli, 2014); (Boelens et al., 1988):

$$\frac{I_{ij}(t)}{I_{ii}(0)} = \frac{I_{ji}(t)}{I_{jj}(0)} = \frac{-\sigma_{ij}}{\lambda_+ - \lambda_-} (\exp\{-\lambda_- t\} - \exp\{-\lambda_+ t\}) \quad (1)$$

59 where  $I_{ii}(t)$  and  $I_{ij}(t)$  represent the peak intensity of the diagonal and the cross-peak in the NOESY  
60 spectrum respectively. The cross-relaxation rate,  $\sigma_{ij}$ , further depends on  $\lambda_{\pm}$  which are a function of auto-  
61 relaxation rates of the two spins,  $\rho_i$  and  $\rho_j$ .

$$\lambda_{\pm} = \frac{\rho_i + \rho_j}{2} \pm \sqrt{\left(\frac{\rho_i - \rho_j}{2}\right)^2 + \sigma_{ij}^2} \quad (2)$$

The diagonal intensities can be approximated by a single-exponential decay, completely independent of  
the auto- and cross-relaxation rates of the other spin:

$$I_{ii}(t) = I_{ii}(0) \exp\{-\rho_i t\} \quad (3)$$

62 Furthermore, under the assumption that  $\rho_i \approx \rho_j = \rho$ , which holds true for small- to medium-sized proteins,  
63 the exponential terms in Equation 1 can be expanded to the second-order as follows:

$$\exp\{-\lambda_{\pm} t\} = \exp\{-(\rho \pm \sigma)t\} = 1 - (\rho \pm \sigma)t + \frac{(\rho \pm \sigma)^2 t^2}{4} \dots \quad (4)$$

Combining Equations 1, 3 and 4, the following expression can be obtained:

$$\boxed{\frac{I_{ij}(t)}{I_{ii}(t)} = -\sigma_{ij} t} \quad (5)$$

64 This straightforward expression relates the cross-peak and diagonal intensities at mixing time,  $t$ , to the  
65 cross-relaxation rate. These quantities can be directly extracted from NOESY spectra recorded at multiple  
66 mixing times and fitted with a simple linear model to compute the cross-relaxation rate. This forgoes the  
67 need for invoking the ENORA module to fit the NOE build-ups. More importantly, it produces more accurate  
68 rates as it only involves directly fitting the experimentally-derived peak build-up intensities once. With the  
69 standard approach used in ENORA, the diagonal intensities are fitted in accordance with Equation 3 to  
70 extrapolate the auto-relaxation rate,  $\rho_i$  and the initial magnetisation,  $I_{ii}(0)$ . The error introduced to these  
71 quantities by imprecise fitting of Equation 3 and low SNR of diagonal peaks is propagated to Equations 1 and  
72 2, which are used to determine  $\sigma_{ij}$ . Furthermore, the imbalance inherent to the F1- $^{15}\text{N}$ ,  $^{13}\text{C}$ -filtered [ $^1\text{H}$ ,  $^1\text{H}$ ]-  
73 NOESY experiment and the missing  $\rho_i$  contributes to the relative error. This error is also compounded in the  
74 eNORA approach as the peak intensity data is transformed and used in multiple fitting equations.

75 The rates determined with the new method proposed here using Equation 5 is termed diagonal-  
76 normalised NOEs. However, there is a level of uncertainty still attached to the restraints extracted via  
77 this method because of the assumption,  $\rho_i = \rho_j$ , especially for large ligand-protein complexes with weak  
78 binding affinities, as  $\rho_j$  might be an order of magnitude above  $\rho_i$ .

79 A simple test was performed to quantify the uncertainty introduced by the above assumption to the  
80 extracted distances. It involved taking artificial distances (3 Å and 5 Å) between two spin pairs followed by  
81 back calculating the value of the respective cross-relaxation rates. The obtained rates were fed to Equations  
82 1 and 2 with varying assumptions of the values of the auto-relaxation rates ( $\rho_j$  and  $\rho_i$ ). The ratios of  
83 magnetisation transfer  $\frac{I_{ij}(t)}{I_{ii}(t)}$  were obtained at identical mixing times [40, 60, 90 and 120 ms], as used by Torres  
84 et al. (Torres et al., 2020) and fitted according to the Equation 5 in an attempt to reproduce the artificial  
85 distances.

86 The results of the test are detailed in Figure A1 in the Appendix. At the ratio of  $\frac{\rho_j}{\rho_i} = 10$ , the highest  
87 measured ratio, generally expected for the complex of a large protein and a small ligand, our method was  
88 able to reproduce the inter-molecular distance with an accuracy of 12.45% for both 3 Å and 5 Å. Hence, we  
89 propose a distance accuracy of  $\pm \sim 10\%$  for our approach. This distance accuracy lies between distances  
90 derived from bi-directional eNOEs (0%) and uni-directional eNOEs (20%) (Strotz et al., 2015).



91 3 RESULTS AND DISCUSSION

92 In order to evaluate the accuracy of the distance extraction method of diagonal-normalised NOEs the  
93 PIN1-Compound 1 complex introduced above is used. All the NMR experiments on the PIN1-Compound 1  
94 complex were conducted and the subsequent resonance assignments were performed by Torres et al (Torres  
95 et al., 2020) (co-authors in this study). They resolved the structure of the binding pocket using NMR<sup>2</sup> on  
96 the inter-molecular, uni-directional, eNOE-derived distance restraints which have an expected accuracy of  
97 20% (Strotz et al., 2015). In this work, we have used their data, recorded on <sup>15</sup>N/<sup>13</sup>C-filtered [<sup>1</sup>H,<sup>1</sup>H]-NOESY  
98 spectra, to evaluate the performance of the diagonal-normalised eNOE analysis as compared to the the  
99 standard eNOE approach (Vögeli et al., 2009); (Vögeli, 2014).

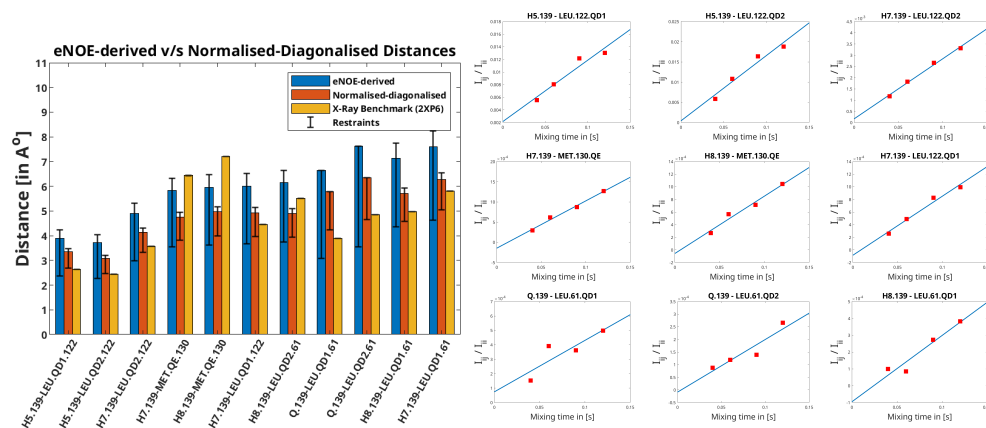


Figure 1: (Left) Distances extracted from F1-<sup>[15</sup>N,<sup>13</sup>C]-filtered [<sup>1</sup>H,<sup>1</sup>H]-NOESY using the eNOE (blue) and diagonal-normalised approach (red) compared to the benchmark X-ray structure. The bars denote the distances that arise from the cross-relaxation rates from the complex of PIN1 with Compound 1, as given in (Torres et al., 2020). The bars in yellow represent the distances back-calculated from the X-ray structure (2XP6) (Potter et al., 2010). The error bars denote the upper and lower limit restraints produced in CYANA (Güntert and Buchner, 2015) for the extracted distances. A tolerance of 20% and 10% was taken and for the eNOE and the diagonal-normalised approach extracted distances respectively. (Right) The ratio of NOE buildups to the corresponding diagonal peak intensities plotted against mixing time for the PIN1-Compound 1 complex for the diagonal-normalised approach. The data points were fitted using a linear least square fitting model in MATLAB (MATLAB, 2018). The slope denotes the cross-relaxation rate of the given peak, as per Equation 5.

100 Apart from being more time-efficient and intuitive, this method should also provide more accurate  
101 distances, as discussed in the Theory section. The NOE build ups plots, fit linearly according to Equation  
102 5, are depicted in Figure 1 (right). The linear fits mostly tend to zero when mixing time is zero and the  
103 experimental data fits well even at longer mixing times for all cross-peaks. This indicates a lack of significant  
104 spin diffusion contribution. Moreover, it is easier to detect spin diffusion with this method compared to the  
105 standard approach using eNORA, as it manifests itself as non-linearity in the fitted data. This difference is  
106 illustrated in Figure A2 in the Appendix.

107 The derived distance restraints are also plotted against the conventional eNOE-derived distance restraint  
108 and the distances back-calculated from the benchmark X-ray structure (2XP6) (Potter et al., 2010) in Figure 1  
109 (left) (The protons were added to the X-ray structure in CYANA (Güntert and Buchner, 2015)). Indeed, the  
110 diagonal-normalised distance restraints better resemble the ones from the X-ray structure (mean difference  
111 in the distances being  $1.04 \pm 0.65 \text{ \AA}$ ) than the ones from the standard approach (mean difference in the  
112 distances being  $1.57 \pm 0.73 \text{ \AA}$ ). The only exceptions being the distances that include the protons from the



113 solvent-exposed Methionine 130. The floppy nature of this region of the binding pocket is predicted to give  
114 minimal distance data.

115 The inter-molecular distances obtained from the PIN1-Compound 1 complex through the conventional  
116 eNORA-based method and the diagonal-normalised approach are plotted in Figure 1. The plots illustrate  
117 that the restraints obtained via the latter are tighter by 0.4-1.2 Å. The source of this difference, as discussed  
118 in the Theory section, arises from the inherent complexity involved in extracting distances from a filtered  
119 2D-NOESY spectrum.

120 To evaluate the 10% error estimate deduced in the Theory section further and to study the impact of the  
121 diagonal-normalised distance restraints on NMR<sup>2</sup> structure determination, NMR<sup>2</sup> structures of the complex  
122 PIN1-Compound 1 were calculated with varying degree of precision of the diagonal-normalised distance  
123 restraints (i.e. 0%, 5%, 10%, and 20%) (Table 1). The restraints were input in the NMR<sup>2</sup> algorithm and the  
124 output structures were compared to the structure determined in (Torres et al., 2020) using standard eNOEs.

125 The NMR<sup>2</sup> program screens all potential combinations of methyl groups in protein and protons on the  
126 ligand and calculates the complex structure for all of the possibilities without needing protein assignment.  
127 The success of an NMR<sup>2</sup> run lies in it being able to discriminate between all the possible structures and  
128 pinpoint the right pose of ligand in the binding pocket. This is especially difficult for small fragments like  
129 Compound 1, with only 5 distinct protons/methyl groups.

Table 1: Table detailing the results of NMR<sup>2</sup> calculations with distance restraints extracted from eNOE and diagonal-normalised method with varying values of errUni in CYANA.

Method Used	Precision (in % of the given distance) <sup>1</sup>	Does the structure converge up to TF = 2 Å <sup>2</sup> ? (Yes/No) <sup>2</sup>	Target Function of 4 lowest energy conformers (in Å <sup>2</sup> )	Total number of degenerate lowest energy conformers	RMSD w.r.t to the benchmark (2XP6) (in Å <sup>2</sup> )
eNORA-based	20%	Yes	[ 0, 0, 0, 0 ]	10+	3.63
Diagonal-Normalised	20%	Yes	[ 0, 0, 0, 0 ]	5	2.17
Diagonal-Normalised	10%	Yes	[ 0.03,0.12,0.20,0.73 ]	1	1.68
Diagonal-Normalised	≤ 5%	No	–	–	–

<sup>1</sup>A precision of x% dictates the value of upper limit and lower limit distance restraints with the upper limit distance restraint being (1+x%)\*(extracted distance) and the lower limit distance restraint being (1-x%)\*(extracted distance).

<sup>2</sup> A target function of less than 2 Å<sup>2</sup> within NMR<sup>2</sup> is considered a successful structure determination (Orts and Riek, 2020).

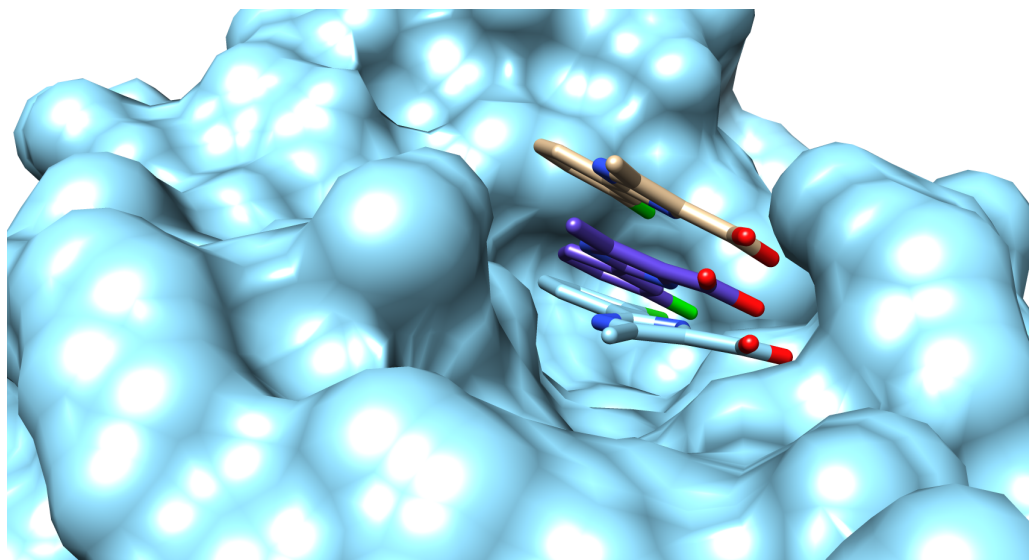


Figure 2: Surface representation of the binding pocket of PIN1 with Compound 1. Coloured in cyan is the surface of the structure determined by X-ray crystallography studies (2XP6) (Potter et al., 2010). Coloured in brown is the structure determined by Torres et al. (Torres et al., 2020) with a distance precision of 20% using the standard ENORA approach and coloured in purple is the structure determined by NMR<sup>2</sup> calculations using the distances extracted via the diagonal-normalised approach with a precision of 10%. The nitrogen, oxygen and chlorine atoms on the ligand are coloured blue, red and green respectively.

130 Table 1 outlines the details of the structure calculation test. The restraints obtained through the eNORA-  
131 based method were not good enough and gave rise to more than 10 degenerate structures with a Target  
132 Function (TF) of  $0 \text{ \AA}^2$ , meaning that all experimental distance restraints were fulfilled without inconsis-  
133 tency/error in any of the 10 degenerate structures. The structure in which the ligand has the same orientation  
134 inside the binding pocket, as the benchmark X-ray structure (2XP6) (Potter et al., 2010), has an RMSD of  
135  $3.63 \text{ \AA}$  with respect to the X-ray structure (2XP6). Using the diagonal-normalised distance determination  
136 procedure with a precision of 20%, a better performance is observed with only 5 degenerate structures with  
137 a TF of  $0 \text{ \AA}^2$ , which included the complex structure with Compound 1 in the right pose (RMSD of  $2.17 \text{ \AA}$ ).  
138 For the anticipated precision of the distance restraints of 10%, the calculation produced only one structure  
139 with a TF =  $0.03 \text{ \AA}^2$ , which shows the same orientation as the crystal structure with an RMSD of  $1.68 \text{ \AA}$ . This  
140 structure superimposes well with the benchmark structure, as shown in Figure 2. A visual inspection of  
141 the binding pocket illustrated in Figure 2 shows that the ligand appears deeper in the binding pocket and  
142 better aligned with the crystal structure compared to the structure obtained by traditional, eNORA-based  
143 NMR<sup>2</sup>. For a distance precision of 5% and below, the calculations did not converge to structures that fulfil  
144 the experimental restraints and produce structures below the hard limit of TF  $< 20 \text{ \AA}^2$ . This is expected  
145 since the distance restraints are not of the quality of bidirectional restraints due to the assumption  $\rho_i = \rho_j$ , the  
146 lack of spin diffusion correction and other restrictions inherent to the NMR<sup>2</sup> protocol, such as the use of a  
147 previously determined protein structure and combining X-ray and NMR data.

148 The strength of this approach lies in distinguishing the correct pose of a weak-binding, low molecular  
149 weight ligands which gives very few inter-molecular NOEs inside the binding pocket of a larger proteins.  
150 Nevertheless, this approach was also tested on the protein-ligand complex of HDM2, a human oncogenic  
151 protein, with caylin-1, which presents abundant inter-molecular NOEs. The traditional eNORA-based NMR<sup>2</sup>  
152 was successful in characterising the structure of protein-ligand interaction site (7QDQ), as shown in the



4 MATERIALS AND METHOD 7

153 work of Mertens et al. (Mertens et al., 2022). With othe diagonal-normalised approach at 10% precision,  
154 we obtained the same pose of caylin-1 in the HDM2 binding site, as Mertens et al., with a TF of 1.52 Å<sup>2</sup>  
155 and RMSD between the two structures being 0.81 Å (refer to Figure A3 in the Appendix). Furthermore,  
156 the calculations made with 15% and 20% precision also matched the predictions of traditional NMR<sup>2</sup> in  
157 identifying the right structure. This is further evidence that our approach can at least match the predictions  
158 of traditional NMR<sup>2</sup> in the case of strong binders and possibly exceed them in the case of weak binders with  
159 less NOEs.

160 To sum up, this work proposes an intuitive and time-efficient, alternative method to extract precise  
161 distance restraints from a series of filtered-NOESY spectra, that gives, in the system studied, an accurate  
162 NMR<sup>2</sup> structure of the protein-ligand interaction site.

163 4 MATERIALS AND METHOD

164 No new material was prepared for the sake of this work. The protocol to express and purify the protein and  
165 the ligand and to mix them afterwards is detailed in (Torres et al., 2020).

166 No new NMR experiments were conducted for this work either. The peak intensities from the spectra  
167 acquired by Torres et al. were extracted via ccpNMR (Skinner et al., 2016). The intensities were later fit to  
168 acquire the rates in the MATLAB Software suite (MATLAB, 2018). The structure calculation were performed  
169 by NMR<sup>2</sup> program through CYANA (Güntert and Buchner, 2015). All the structures were displayed and  
170 overlaid over each other using the Chimera molecular visualisation tool (Pettersen et al., 2004).

171 5 ACKNOWLEDGEMENT

172 We would like to thank the Swiss National Foundation for financial support through the grant number  
173 310030\_192646.

174 6 CONFLICT OF INTEREST

175 No conflict of interest.

176 7 DATA AVAILABILITY

177 All relevant data can be obtained upon request.

178 BIBLIOGRAPHY

179 Boelens, R., Koning, T. M. G., and Kaptein, R.: Determination of biomolecular structures from proton-  
180 proton NOE's using a relaxation matrix approach, *Journal of Molecular Structure*, 173, 299–311, doi:  
181 10.1016/0022-2860(88)80062-0, URL <https://www.sciencedirect.com/science/article/pii/0022286088800620>,  
182 1988.

183 Güntert, P. and Buchner, L.: Combined automated NOE assignment and structure calculation with CYANA,  
184 *Journal of Biomolecular NMR*, 62, 453–471, doi:10.1007/s10858-015-9924-9, URL <https://doi.org/10.1007/s10858-015-9924-9>, 2015.

186 Kalk, A. and Berendsen, H. J. C.: Proton magnetic relaxation and spin diffusion in proteins, *Journal of*  
187 *Magnetic Resonance* (1969), 24, 343–366, doi:10.1016/0022-2364(76)90115-3, URL <https://www.sciencedirect.com/science/article/pii/0022236476901153>, 1976.





- 189 Keepers, J. W. and James, T. L.: A theoretical study of distance determinations from NMR. Two-  
190 dimensional nuclear overhauser effect spectra, *Journal of Magnetic Resonance* (1969), 57, 404–426, doi:  
191 10.1016/0022-2364(84)90257-9, URL <https://www.sciencedirect.com/science/article/pii/0022236484902579>,  
192 1984.
- 193 MATLAB: 9.7.0.1190202 (R2018b), The MathWorks Inc., Natick, Massachusetts, 2018.
- 194 Mertens, V., Abi Saad, M. J., Coudevylle, N., Wälti, M. A., Finke, A., Marsh, M., and Orts, J.: Elucidation of a  
195 nutlin-derivative—HDM2 complex structure at the interaction site by NMR molecular replacement: A  
196 straightforward derivation, *Journal of Magnetic Resonance Open*, 10-11, 100 032, doi:10.1016/j.jmro.2022.  
197 100032, URL <https://www.sciencedirect.com/science/article/pii/S2666441022000024>, 2022.
- 198 Orts, J. and Riek, R.: Protein–ligand structure determination with the NMR molecular replacement  
199 tool, *NMR2, Journal of Biomolecular NMR*, 74, 633–642, doi:10.1007/s10858-020-00324-y, URL <https://doi.org/10.1007/s10858-020-00324-y>, 2020.  
200
- 201 Orts, J., Wälti, M. A., Marsh, M., Vera, L., Gossert, A. D., Güntert, P., and Riek, R.: NMR-Based Determination  
202 of the 3D Structure of the Ligand–Protein Interaction Site without Protein Resonance Assignment, *Journal*  
203 *of the American Chemical Society*, 138, 4393–4400, doi:10.1021/jacs.5b12391, URL [https://doi.org/10.1021/](https://doi.org/10.1021/jacs.5b12391)  
204 [jacs.5b12391](https://doi.org/10.1021/jacs.5b12391), publisher: American Chemical Society, 2016.
- 205 Pettersen, E. F., Goddard, T. D., Huang, C. C., Couch, G. S., Greenblatt, D. M., Meng, E. C., and Ferrin, T. E.:  
206 UCSF Chimera—A visualization system for exploratory research and analysis, *Journal of Computational*  
207 *Chemistry*, 25, 1605–1612, doi:10.1002/jcc.20084, URL [https://onlinelibrary.wiley.com/doi/abs/10.1002/jcc.](https://onlinelibrary.wiley.com/doi/abs/10.1002/jcc.20084)  
208 [20084](https://onlinelibrary.wiley.com/doi/abs/10.1002/jcc.20084), eprint: <https://onlinelibrary.wiley.com/doi/pdf/10.1002/jcc.20084>, 2004.
- 209 Potter, A., Oldfield, V., Nunns, C., Fromont, C., Ray, S., Northfield, C. J., Bryant, C. J., Scrace, S. F., Robinson,  
210 D., Matosova, N., Baker, L., Dokurno, P., Surgenor, A. E., Davis, B., Richardson, C. M., Murray, J. B.,  
211 and Moore, J. D.: Discovery of cell-active phenyl-imidazole Pin1 inhibitors by structure-guided fragment  
212 evolution, *Bioorganic & Medicinal Chemistry Letters*, 20, 6483–6488, doi:10.1016/j.bmcl.2010.09.063, URL  
213 <https://www.sciencedirect.com/science/article/pii/S0960894X10013648>, 2010.
- 214 Skinner, S. P., Fogh, R. H., Boucher, W., Ragan, T. J., Mureddu, L. G., and Vuister, G. W.: CcpNmr  
215 AnalysisAssign: a flexible platform for integrated NMR analysis, *Journal of Biomolecular NMR*, 66,  
216 111–124, doi:10.1007/s10858-016-0060-y, URL <https://doi.org/10.1007/s10858-016-0060-y>, 2016.
- 217 Strotz, D., Orts, J., Minges, M., and Vögeli, B.: The experimental accuracy of the uni-directional exact NOE,  
218 *Journal of Magnetic Resonance*, 259, 32–46, doi:10.1016/j.jmr.2015.07.007, URL [https://www.sciencedirect.](https://www.sciencedirect.com/science/article/pii/S1090780715001597)  
219 [com/science/article/pii/S1090780715001597](https://www.sciencedirect.com/science/article/pii/S1090780715001597), 2015.
- 220 Strotz, D., Orts, J., Chi, C. N., Riek, R., and Vögeli, B.: eNORA2 Exact NOE Analysis Program, *Journal of*  
221 *Chemical Theory and Computation*, 13, 4336–4346, doi:10.1021/acs.jctc.7b00436, URL [https://doi.org/10.](https://doi.org/10.1021/acs.jctc.7b00436)  
222 [1021/acs.jctc.7b00436](https://doi.org/10.1021/acs.jctc.7b00436), publisher: American Chemical Society, 2017.
- 223 Torres, F., Ghosh, D., Strotz, D., Chi, C. N., Davis, B., and Orts, J.: Protein–fragment complex structures  
224 derived by NMR molecular replacement, *RSC Medicinal Chemistry*, 11, 591–596, doi:10.1039/DoMD00068J,  
225 URL <https://pubs.rsc.org/en/content/articlelanding/2020/md/d0md00068j>, publisher: RSC, 2020.
- 226 Vögeli, B.: The nuclear Overhauser effect from a quantitative perspective, *Progress in Nuclear Magnetic*  
227 *Resonance Spectroscopy*, 78, 1–46, doi:10.1016/j.pnmrs.2013.11.001, URL [https://www.sciencedirect.com/](https://www.sciencedirect.com/science/article/pii/S0079656513001003)  
228 [science/article/pii/S0079656513001003](https://www.sciencedirect.com/science/article/pii/S0079656513001003), 2014.
- 229 Vögeli, B., Segawa, T. F., Leitz, D., Sobol, A., Choutko, A., Trzesniak, D., van Gunsteren, W., and Riek,  
230 R.: Exact Distances and Internal Dynamics of Perdeuterated Ubiquitin from NOE Buildups, *Journal of*





BIBLIOGRAPHY 9

- 231 the American Chemical Society, 131, 17 215–17 225, doi:10.1021/ja905366h, URL [https://doi.org/10.1021/  
232 ja905366h](https://doi.org/10.1021/ja905366h), publisher: American Chemical Society, 2009.
- 233 Wälti, M. A. and Orts, J.: The NMR<sub>2</sub> Method to Determine Rapidly the Structure of the Binding  
234 Pocket of a Protein–Ligand Complex with High Accuracy, *Magnetochemistry*, 4, 12, doi:10.3390/  
235 magnetochemistry4010012, URL <https://www.mdpi.com/2312-7481/4/1/12>, number: 1 Publisher: Multi-  
236 disciplinary Digital Publishing Institute, 2018.
- 237 Zwahlen, C., Legault, P., Vincent, S. J. F., Greenblatt, J., Konrat, R., and Kay, L. E.: Methods for Measurement of  
238 Intermolecular NOEs by Multinuclear NMR Spectroscopy: Application to a Bacteriophage N-Peptide/boxB  
239 RNA Complex, *Journal of the American Chemical Society*, 119, 6711–6721, doi:10.1021/ja970224q, URL  
240 <https://doi.org/10.1021/ja970224q>, publisher: American Chemical Society, 1997.

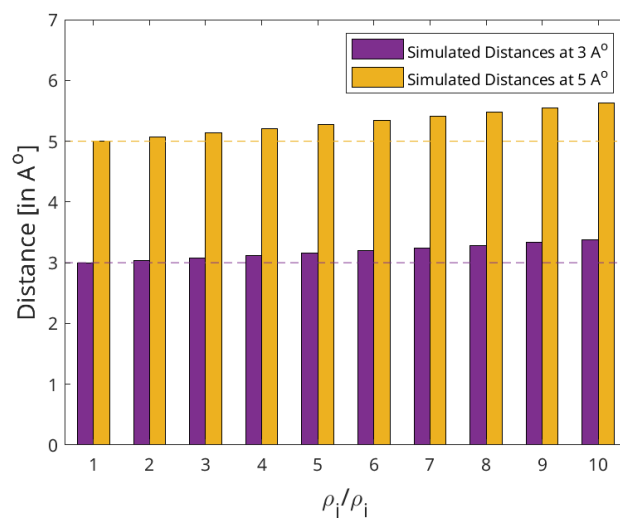


Figure A1: The effect of the relative auto-relaxation rates of the protein and the ligand on the distances extracted via the diagonal-normalised approach. The dotted lines represent the artificial distances 3 Å and 5 Å in purple and yellow respectively. The corresponding bars denote the distances back-calculated using the diagonal-normalised approach from the artificial distances depending on the the relative auto-relaxation rates,  $\rho_i$  and  $\rho_j$ . Each set of distances (bars) are derived through varying assumptions of the values of  $\rho_i$  and  $\rho_j$  with respect to each other ranging from  $\frac{\rho_j}{\rho_i} = [1 \text{ to } 10]$ .

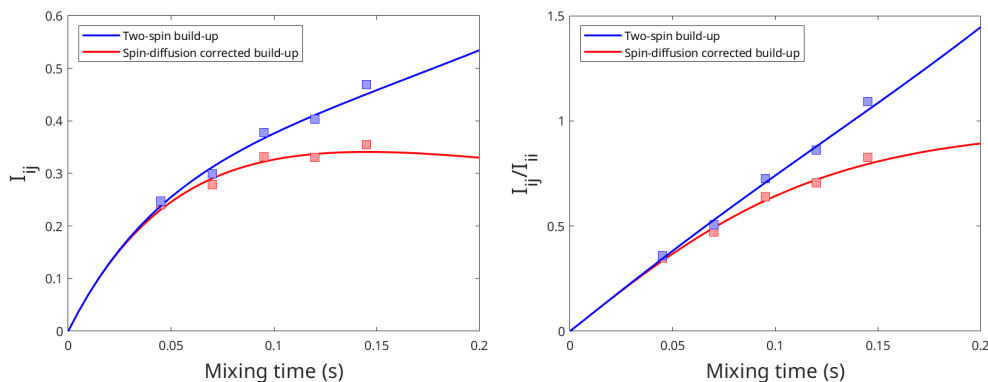


Figure A2: Effect of spin diffusion on the intensity build-up curves produced from eNORA-based approach (left) and diagonal-normalised approach (right). The build-up curves were fitted using artificially simulated peak intensities in a model system. The blue curve represents the intensity build-up in an isolated two-spin system and the red curve represents the same two spins experiencing spin-diffusion due to presence of other spins in the system. The comparison between the plots highlight that it is easier to detect the influence of spin-diffusion with the diagonal-normalised approach (right), as it induces deviation from the expected linear fit.

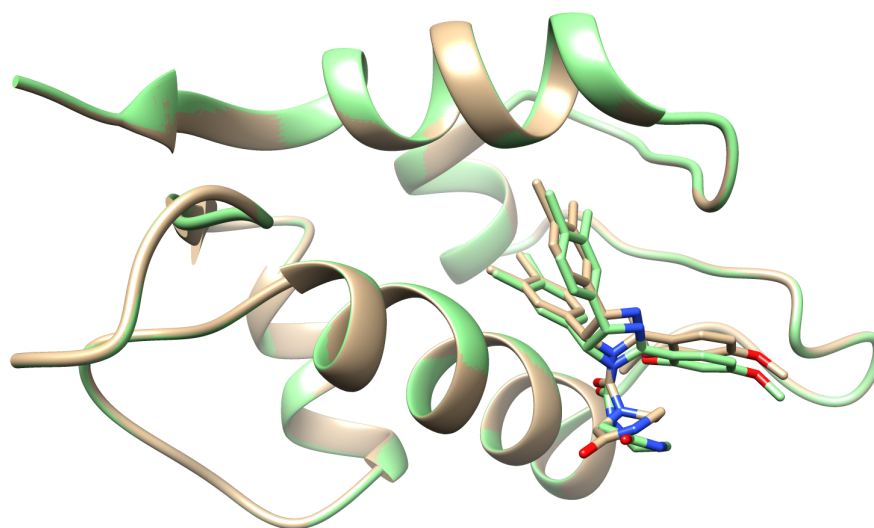


Figure A3: Ribbon representation of the protein, HDM2, with the stick representation of caylin-1 present in the binding pocket. Coloured in brown is the surface of the structure determined by traditional NMR<sup>2</sup> (7QDQ) by Mertens et al. (Mertens et al., 2022). Coloured in green is the structure determined by NMR<sup>2</sup> calculations using the the diagonal-normalised approach with a precision of 10%. The nitrogen and oxygen atoms on the ligand are coloured blue and red respectively.